Numerical and Compact Modelling of Squeeze-Film Damping in RF MEMS Resonators

T. Veijola, Anu Lehtovuori

DTIP of MEMS & MOEMS 9-11 April 2008

Numerical and Compact Modelling of Squeeze-film Damping in RF MEMS Resonators

T. Veijola and A. Lehtovuori
Department of Radio Science and Engineering,
Helsinki University of Technology, P.O.Box 3000, FIN-02015 HUT, Finland

Abstract— **Oscillatory gas flow in squeeze-film dampers is studied up to frequencies where the length of the acoustic wave is comparable with the dimensions of the air gap. Damping and spring forces are calculated both numerically and analytically from the linearized 2D Navier-Stokes equations. In addition to the low frequency region of inertialess gas, where the use of the Reynolds equation is limited, the new model considers several additional phenomena. These are the inertia of the gas, the transition from isothermal to adiabatic conditions, and the gap resonances at frequencies where the acoustic wavelength is comparable to the air gap height. Velocity and temperature slip conditions are considered to make the model valid in micromechanical structures where the air gap heights are of the order of a micrometer.**

An approximate compact model is derived combining the low frequency model and the gap resonance model. The accuracy of the compact model is studied by comparing its response to the numerical results calculated with the finite element method. The agreement is very good in a wide frequency band when the ratio of the damper width and the gap height is greater than 10. The numerical study and the compact model are directly applicable in predicting the damping and the resonance frequency shift due to air in RF MEMS resonators having narrow air gap widths and operating at frequencies where the wavelengths become comparable to the flow channel dimensions.

I. Introduction

It has been reported RF MEMS resonators that operate at frequencies up to 1 GHz [1], [2]. Since these devices can operate also at atmospheric pressures, models predicting the quality factor and resonance frequency shift due to air are needed. The challenges in the modelling are the small acoustic wavelengths that might become comparable with the dimension of the damper width and even the air gap height, and the small dimensions of micromechanical devices that invalidate the continuum flow assumptions.

Squeeze-film damping in air gaps of oscillating structures has been traditionally modelled with the Reynolds equation [3], [4]. It considers the viscous gas flow and the compressibility and assumes constant pressure across the air gap. With an effective viscosity, the rarefied gas phenomenon can be considered. This extends the model to be used for micromechanical devices and or low ambient pressure. However, the Reynolds equation is usable only up to a certain frequency where the inertial forces can be neglected (Reynolds number $\ll$ 1). This limitation can be avoided using a modified form of the Reynolds equation considering the inertia in the gap flow [5] together with non-isothermal conditions [6], [7]. This viscoelastic wave propagation model is not directly applicable to model MEMS devices, since it assumes continuum boundary conditions.

When the frequency of the oscillation is so high that the length of the acoustic wave becomes comparable to the height of the air gap, the constant pressure assumption across the air gap breaks down. This situation has been studied and modelled in [8]. The study shows that since the gas is trapped in the gap, it is justified to assume closed damper borders in deriving the model. The analytic model derived in [8] models accurately the damper in the higher frequency region where the air gap resonances occur.

In this paper, numerical simulation of the linearized Navier-Stokes equations are first used to study the oscillating flow in the air gap of a 1D squeeze-film damper in a wide frequency band. Slip velocity and temperature boundary conditions at the surfaces, and zero pressure conditions at the damper borders are applied. A finite element method (FEM) software is used in the study.

Next, reduced linearized Navier-Stokes equations are presented that consider the variable pressure across the air gap to be able to include the gap resonances in the model [8]. The gap resonances are solved at high frequencies and the squeeze film phenomenon is solved at lower frequencies. Then, these results are combined to have a compact approximate model for a wide frequency regime. Finally, the compact model is compared with the numerical model to verify its accuracy.

II. Oscillating gas flow in a squeeze-film damper

A. Topology of the damper

Figure 1 shows the topology of the studied 1D squeeze-film damper. It is assumed that the 3rd dimension l_y is much larger than l_x justifying the study of the 2D gas flow in the cross-section. The gas is bounded by two rigid parallel surfaces, and the upper surface is oscillating with a small amplitude of w_0 in the z direction. Trivial zero-pressure boundary conditions are used at the borders of the damper.

B. Damping and spring forces

The damper is characterized with a mechanical impedance $Z_\mathrm{m} = -\frac{\tilde{F}}{w_0}$, that is calculated from the force $\tilde{F}$ acting on the moving surface having a velocity of w_0 in the z direction.

 ISBN: 978-2-35500-006-5

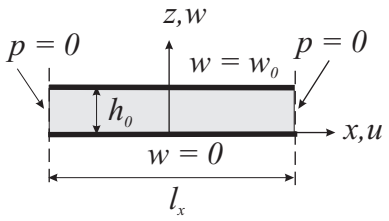

Fig. 1. The cross-section of squeeze-film damper. The y dimension of the damper l_{y} is assumed to me much larger than the x dimension l_{x}.

The damping coefficient c is the real part of Z_{m} and the spring coefficient k is the real part of $\mathrm{i}\omega Z_{\mathrm{m}}$.

C. Characteristic numbers

The behaviour of the flow in a narrow air gap is described by a few characteristic numbers. The Reynolds number $\mathtt{Re}$ (the square of the shear wave number s) is the ratio between inertial and viscous forces: $s^2 = \mathtt{Re} = \omega h_0^2 \rho_0/\eta$, where ρ_0 is the density of the gas, η is the viscosity coefficient, and h_0 is the characteristic height of the air gap.

The reduced frequency $k = \omega h_0/c_0$ is a measure of the ratio between the gap width h_0 and the acoustic wave length. $c_0 = \sqrt{\gamma p_0/\rho_0}$ is the speed of sound in free space, where $\gamma = c_{\mathrm{P}}/c_{\mathrm{V}}$ is the specific heat ratio and p_0 is the ambient pressure. The Prandtl number $\mathtt{Pr}$ characterizes the thermal properties. Here we use the square root of $\mathtt{Pr}$,

$$\phi = \sqrt{\mathtt{Pr}} = \sqrt{\frac{\eta c_{\mathrm{P}}}{\kappa}}, \tag{1}$$

where c_{P} is the specific heat at constant pressure and κ is the thermal conductivity.

A frequency-domain analysis with small perturbation amplitudes is assumed, and the equations are presented in normalized form. The small-amplitude perturbation variables: pressure, temperature and density are specified with

$$\tilde{p} = p_0 + pe^{\mathrm{i}\omega t}, \quad \tilde{T} = T_0 + Te^{\mathrm{i}\omega t}, \quad \tilde{\rho} = \rho_0 + \rho e^{\mathrm{i}\omega t}, \tag{2}$$

respectively.

D. Linearized Navier-Stokes equations

Beltman [6] has derived linearized dimensionless form of the Navier-Stokes equations. The equations are in 2D (y-direction is not considered):

$$\mathrm{i}u = \frac{-g}{k\gamma}\frac{\partial p}{\partial x} + \frac{1}{s^2}\left[g^2\frac{\partial^2 u}{\partial x^2} + \frac{\partial^2 u}{\partial z^2}\right] + \frac{g}{3s^2}\frac{\partial}{\partial x}\left[g\frac{\partial u}{\partial x} + \frac{\partial w}{\partial z}\right] \tag{3}$$

$$\mathrm{i}w = \frac{-1}{k\gamma}\frac{\partial p}{\partial z} + \frac{1}{s^2}\left[g^2\frac{\partial^2 w}{\partial x^2} + \frac{\partial^2 w}{\partial z^2}\right] + \frac{1}{3s^2}\frac{\partial}{\partial z}\left[g\frac{\partial u}{\partial x} + \frac{\partial w}{\partial z}\right] \tag{4}$$

$$g\frac{\partial u}{\partial x} + \frac{\partial w}{\partial z} = -\mathrm{i}k\rho \tag{5}$$

$$p = \rho + T \tag{6}$$

$$\mathrm{i}T = \frac{1}{s^2\phi^2}\left[g^2\frac{\partial^2 T}{\partial x^2} + \frac{\partial^2 T}{\partial z^2}\right] + \mathrm{i}\frac{\gamma - 1}{\gamma}p, \tag{7}$$

where u and w are velocity components in the x and z directions, respectively. The equations are in normalized form such that velocities u and w are normalized to the speed of sound c_0 and the dimensions x and z are normalized with the characteristic dimensions l_{x} and h_0, respectively. p, ρ, and T represent small relative variations around p_0, ρ_0 and T_{A}, respectively. The narrowness of the gap is $g = h_0/l_x$.

E. Numerical modeling

To study gas flow in the air gap, pressure, velocity, and temperature of the 1D-damper in Fig. 1 are simulated with a FEM solver for visco-acoustic flow [9] in multiphysical FEM software ELMER [10]. It solves linearized Navier-Stokes equation presented in (3)-(7) as a function of frequency.

In this study, parameters for air at standard atmosphere conditions are used, see Table I. The air gap height is $h_0 = 1\mu$m and the length is $l_x = 5\mu$m. The upper surface oscillates in the z-direction with a constant velocity amplitude of 1 m/s ($w_0 = 1$).

TABLE I

GAS PARAMETERS USED IN THE SIMULATIONS

Symbol	Description	Value	Unit
p_0	pressure	101.3	10^3 N/m^2
T_{A}	temperature	300	K
η	viscosity coefficient	18.5	10^{-6} N s/m^2
ρ_0	density of air	1.155	kg/m^3
c_{P}	specific heat	1.01	10^3 J/kg/K
γ	specific heat ratio	1.4	
κ	heat conductivity	0.025	W/m/K
λ	mean free path (17)	68.22	10^{-9} m
α	accommodation coefficient	1.0	
α_{T}	thermal acc. coefficient	1.0	

To demonstrate the trapping of the gas in the air gap at high frequencies, Fig. 2 shows forces acting on the upper surface as a function of frequency in two cases. First, the borders are assumed to be open (zero pressure) and then they are assumed to be closed (zero velocity). The amplitude responses are identical above a certain frequency indicating that at high frequencies the flow velocity in the x direction becomes insignificant. Hence, at high frequencies the gas is trapped in the gap corresponding the closed border assumption, even for open border conditions.

Figure 3 shows simulated pressure, velocity, and temperature amplitude distributions for the open border case at certain frequencies, represented with verticals in Fig. 2. These frequencies represent different flow regions that will be studied closer. Resonances occur both in the x and y directions: squeeze film phenomenon at lower frequency when the gas flows out from the gap and gap resonances at higher frequency when the gas is trapped in the gap.

(a) Viscous flow region: pressure is constant across the gap, and isothermal conditions ($T = 0$).

 ISBN: 978-2-35500-006-5

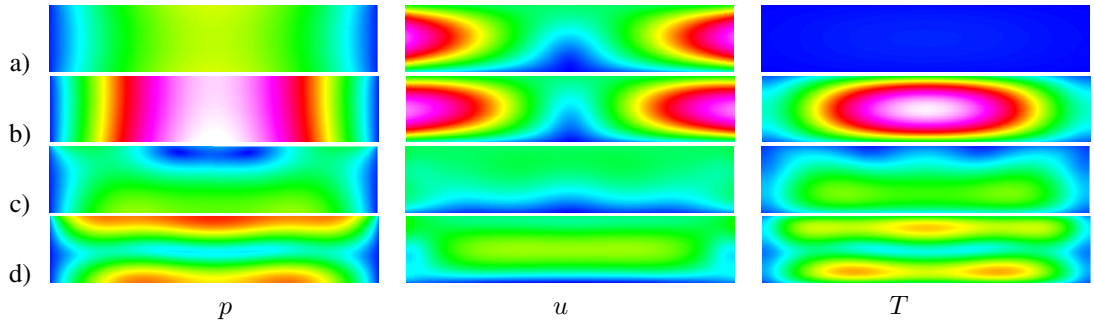

Fig. 3. Amplitude profiles of pressure p, velocity u, and temperature T at different frequencies. a) $f = 1\,\text{MHz}$, b) $f = 30\,\text{MHz}$, c) $f = 100\,\text{MHz}$, d) $f = 180\,\text{MHz}$

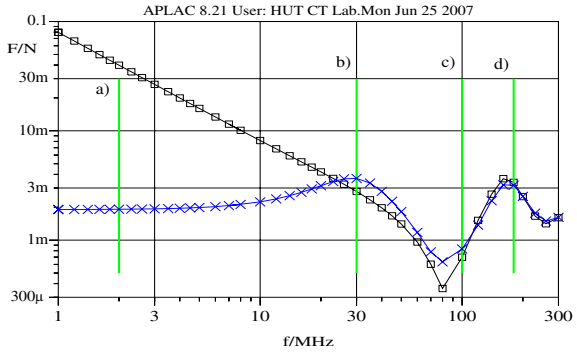

Fig. 2. Simulated force amplitude on the upper surface for open (×) and closed (□) ends cases.

(b) First resonance in the x direction. Its frequency $f_{\text{x},N}$ is determined by the wave propagation velocity in the x direction and the length of the structure. The squeeze film resonant frequencies are

$$f_{\text{x},N} \approx \frac{N c_{\text{e}}}{4L}, \quad N = 2, 4, \ldots \tag{8}$$

where L is the characteristic length of the damper and c_{e} is the effective speed of sound in the x-direction. The temperature profile in Fig. 3 indicates non-isothermal conditions.

(c) First (anti)resonance $f_{\text{z},1}$ in the x-direction: pressure is not constant across the gap, small velocity (trapped situation). The Nth air gap resonance frequency is

$$f_{\text{z},N} \approx \frac{N c_0}{4h_0}, \quad N = 1, 2, 3, \ldots \tag{9}$$

where h_0 is the height of the gap. Odd values of N give antiresonances, while even values of N give resonances. Air gap resonances occur at clearly higher frequency than the squeeze film resonance if the gap is narrow ($h_0 \ll l_{\text{x}}$). Non-isothermal conditions.

(d) 2nd gap resonance $f_{\text{z},2}$: pressure, velocity and temperature vary mainly in the z-direction, practically adiabatic conditions.

F. Reduced equations for the approximative model

In order to derive the compact model, a reduced set of NS-equations is needed. The complete set of 2D equations (3)-(7) will be reduced by removing insignificant terms. Equation (3) is first written in the following form:

$$\mathrm{i}u = -\frac{g}{k\gamma}\frac{\partial p}{\partial x} + \frac{4g^2}{3s^2}\frac{\partial^2 u}{\partial x^2} + \frac{1}{s^2}\frac{\partial}{\partial z}\left[\frac{\partial u}{\partial z} + \frac{g}{3}\frac{\partial w}{\partial x}\right] \tag{10}$$

Since velocity u varies less in the x-direction than in the z-direction, and g is small, term $\partial^2 u/\partial x^2$ can be ignored. Also, due to translational velocity excitation, the term $\partial w/\partial x$ is very small and is ignored here. At low frequencies, k is small and (4) reduces simply to $\partial p/\partial z = 0$. At high frequencies $\partial^2 w/\partial x^2$ is small due to the excitation, and $\partial u/\partial x$ is small in (4) due to the trapped situation. Temperature variations are slower in the x direction than in the z direction, and g is small in (7), making the term $\partial^2 T/\partial x^2$ to vanish. The reduced equations are:

$$\mathrm{i}u = -\frac{g}{k\gamma}\frac{\partial p}{\partial x} + \frac{1}{s^2}\frac{\partial^2 u}{\partial z^2} \tag{11}$$

$$\mathrm{i}w = -\frac{1}{k\gamma}\frac{\partial p}{\partial z} + \frac{4}{3s^2}\frac{\partial^2 w}{\partial z^2} \tag{12}$$

$$g\frac{\partial u}{\partial x} + \frac{\partial w}{\partial z} = -\mathrm{i}k\rho \tag{13}$$

$$p = \rho + T \tag{14}$$

$$\mathrm{i}T = \frac{1}{s^2\phi^2}\frac{\partial^2 T}{\partial z^2} + \mathrm{i}\frac{\gamma - 1}{\gamma}p. \tag{15}$$

These equations are identical with the "narrow gap" equations specified in [6], but they include an additional equation (12).

The strategy to have an approximate solution for the equations above is the following. First, the equations are further reduced to have the trapped air situation. This is accomplished assuming flow in the z direction only, that is, $u(x) = 0$, and solving the velocity profile $w(z)$. Next, the narrow gap situation is assumed ignoring (4), and a differential equation for the pressure distribution is derived. Finally, the flow profile $w(z)$ is inserted in the differential

 ISBN: 978-2-35500-006-5

equation that is solved for perpendicular motion and zero pressure boundary conditions.

G. Air gap resonance region

It was shown numerically that at high frequencies the gas is trapped in the air gap, and moves only in the z direction. The problem has been studied closer in [8], where both a simplified model with adiabatic conditions and a complete model are given.

H. Squeeze film damping region

Next, the lower frequency (squeeze-film damping) region is studied in order to derive the compact model for the mechanical impedance of the damper. This is accomplished by using the equations (11)-(15) for narrow gap problems, that is, Eq, (12) will be ignored in the following analysis.

The solution strategy is similar to the one in [6], but here the slip velocity and temperature conditions are used instead of the continuum boundary conditions.

The slip boundary conditions for the gas velocity u and the temperature T are used at the surfaces:

$$u = \mp K_\mathrm{s} \left.\frac{\partial u}{\partial z}\right|_{z=0,z=1} \qquad T = \mp K_\mathrm{T} \left.\frac{\partial T}{\partial z}\right|_{z=0,z=1} \tag{16}$$

The Knudsen number $K_\mathrm{n} = \lambda/h_0$ is a measure of gas rarefaction. It is a ratio between the mean free path λ and the nominal displacement h_0. Here, the mean free path is specified as

$$\lambda = \frac{\eta}{\rho_0}\sqrt{\frac{\pi}{2RT_0}} \tag{17}$$

where $R = c_\mathrm{V} - c_\mathrm{P}$. In this paper, we use the quantity $K_\mathrm{s} = \sigma_\mathrm{P}\lambda/h_0$ as a measure of the rarefaction instead of K_n. Since λ is inversely proportional to pressure, K_s increases as the pressure drops below the ambient pressure. In this paper $\sigma_\mathrm{P} = 1$ is assumed.

K_T is the "thermal Knudsen number" [11]

$$K_\mathrm{T} = \frac{2-\alpha_\mathrm{T}}{\alpha_\mathrm{T}}\left[\frac{2\gamma}{\gamma+1}\right]\frac{K_\mathrm{n}}{\phi^2}, \tag{18}$$

where α_T is the energy accommodation coefficient and γ is the specific heat ratio.

Since the pressure was assumed to be constant on a cross section, p and $\partial p/\partial x$ are independent of z in (11) and (15). Therefore, the temperature can be solved from (15). Solution is searched in form $T(z) = b + c\cosh[\xi(z-\frac{1}{2})]$ and applying boundary conditions in (16) results in

$$T = \frac{\gamma-1}{\gamma} pA(\phi s, K_\mathrm{T}, z), \tag{19}$$

where the temperature profile is described with

$$A(s, K_\mathrm{s}, z) = 1 - \frac{\cosh[\sqrt{\mathrm{i}}s(z-\frac{1}{2})]}{\cosh(\sqrt{\mathrm{i}}s/2) + \sqrt{\mathrm{i}}sK_\mathrm{s}\sinh(\sqrt{\mathrm{i}}s/2)}. \tag{20}$$

Remark, that although the pressure is assumed to be constant in z-direction, the temperature depends on z. Next, the density is solved from (14) resulting in $\rho = p/m(\phi s, K_\mathrm{T}, z)$ where

$$m(\phi s, K_\mathrm{T}, z) = \left[1 - \frac{\gamma-1}{\gamma}A(\phi s, K_\mathrm{T}, z)\right]^{-1}. \tag{21}$$

Equation (11) has the same form as (15) for temperature and u can be solved when $p = p(x)$ yielding

$$u = \frac{\mathrm{i}g}{k\gamma}\frac{\partial p}{\partial x}A(s, K_\mathrm{s}, z). \tag{22}$$

The differential equation for the pressure distribution in the x-direction is derived from (13) by averaging the velocity u and density ρ across the gap:

$$g\int_0^1 \frac{\partial u}{\partial x}\,\mathrm{d}z + \mathrm{i}k\int_0^1 \rho\,\mathrm{d}z = -\left.\frac{\partial w}{\partial z}\right|_{z=1}. \tag{23}$$

Since the mechanical impedance is specified at $z = 1$, the term in the right hand side has not been averaged across the gap. Instead of the average velocity in the z direction, the excitation velocity at the upper surface ($z = 1$) is used here.

Inserting u from (22) and ρ from (14) into (23) gives a general frequency-domain model for 1D air gaps

$$\frac{g^2B(s, K_\mathrm{s})}{\mathrm{i}k\gamma}\frac{\partial^2 p(x)}{\partial x^2} - \frac{\mathrm{i}k}{n(\phi s, K_\mathrm{T})}p(x) = \left.\frac{\partial w}{\partial z}\right|_{z=1}. \tag{24}$$

where

$$\begin{aligned} B(s, K_\mathrm{s}) &= \int_0^1 A(s, K_\mathrm{s}, z)\,\mathrm{d}z \\ &= \frac{\sqrt{\mathrm{i}}s - (2 - \mathrm{i}s^2K_\mathrm{s})\tanh(\sqrt{\mathrm{i}}s/2)}{\sqrt{\mathrm{i}}s + \mathrm{i}s^2K_\mathrm{s}\tanh(\sqrt{\mathrm{i}}s/2)} \end{aligned} \tag{25}$$

and the similar integration of $m(\phi s, K_\mathrm{T}, z)$ gives the polytropic constant

$$n(\phi s, K_\mathrm{T}) = \left[1 - \frac{\gamma-1}{\gamma}B(\phi s, K_\mathrm{T})\right]^{-1}. \tag{26}$$

The function n is the result of thermal effects. It is generally complex-valued signifying a phase shift between the pressure and density perturbation. Hence, it models the losses due to gas compressibility that are important in the transition regime when conditions change from isothermal to adiabatic. At low frequencies ($\phi s \ll 1$), the flow is isothermal leading to $n = 1$ and at high frequencies ($\phi s \gg 1$), $B(s, K_\mathrm{s})$ approaches 1 and $n \to \gamma$ (adiabatic conditions).

Equation (24) is solved with trivial pressure boundary conditions $p(\pm\frac{1}{2}) = 0$. The solution is searched in form $p(x) = b\cosh(cx) + d$, yielding

$$p(x) = \frac{n(\phi s, K_\mathrm{T})}{\mathrm{i}k}\left[\frac{\cosh(\sqrt{\mathrm{i}\sigma_\mathrm{c}}x)}{\cosh(\sqrt{\mathrm{i}\sigma_\mathrm{c}}/2)} - 1\right]\left.\frac{\partial w}{\partial z}\right|_{z=1}, \tag{27}$$

 ISBN: 978-2-35500-006-5

where σ_c is the complex squeeze number

$$\sigma_c = \frac{ik^2\gamma}{g^2 B(s,K_s)n(\phi s,K_T)} = \frac{is^2\sigma}{12B(s,K_s)n(\phi s,K_T)}, \quad (28)$$

where the traditional squeeze number σ is defined as $\sigma = 12\eta l_x^2\omega/(p_0 h_0^2)$. It specifies the ratio between the spring force due to the gas compressibility and the force due to the viscous flow.

I. Complete approximate model

The resulting force acting on the surface is

$$\begin{aligned} F &= \int_{-1/2}^{1/2}\int_{-1/2}^{1/2} p(x)\,dx\,dy \quad (29)\\ &= \frac{n(\phi s,K_T)}{ik}\left[\frac{2}{\sqrt{i\sigma_c}}\tanh(\sqrt{i\sigma_c}/2)-1\right]\left.\frac{\partial w}{\partial z}\right|_{z=1}, \end{aligned}$$

where the velocity excitation is calculated when $z = 1$.

In (32) the last derivative is still unknown. Two different velocity functions $w(z)$ has been derived in [8] assuming closed damper boundaries and gap resonances.

The simpler model gives at $z = 1$

$$\left.\frac{\partial w}{\partial z}\right|_{z=1} = \frac{w_0 q}{\tanh(q)} \quad (30)$$

and the more complicated model gives

$$\left.\frac{\partial w}{\partial z}\right|_{z=1} = C_1 r_1 e^{r1} + C_2 r_2 e^{r2} + C_3 r_3 e^{r3} + C_4 r_4 e^{r4}, \quad (31)$$

respectively. Coefficients C_i and r_i are given in the Appendix.

The un-normalized force becomes

$$\tilde{F} = -\frac{l_x l_y n(\phi s,K_T)p_0}{i\omega h_0}\left[\frac{2}{\sqrt{i\sigma_c}}\tanh(\sqrt{i\sigma_c}/2)-1\right]\left.\frac{\partial w}{\partial z}\right|_{z=h_0}. \quad (32)$$

Equation (32) is the complete model to calculate the force as a function of frequency for a velocity excitation. The damping force is the real part of $\tilde{F}$.

III. Results

In the following, the results of the compact model are compared to numerical FEM simulations which can be considered as exact results. Then, the importance of the included features in the compact model is studied by comparing the responses of published models in a wide frequency band. In the following figures, magnitude or real part is denoted with $\times$ at left-side axis and phase (or spring coefficient) with $\square$ at right-side axis.

A. 2D FEM Simulations

FEM simulations were performed with a solver for dissipative acoustic flow [9] included in Elmer [10] software. The solver gives the results directly at specified frequencies. Since the compact model considers a 1D damper, 2D FEM simulations are sufficient here. A sinusoidal velocity amplitude of 1 m/s was used as the excitation. The symmetry of the structure was utilized in the FEM simulations; only a half of the air gap was simulated. Slip velocity and temperature conditions were applied, and the thermal boundary conditions were set for ideally thermally conducting surfaces. Boundary conditions $p(\pm l_x/2) = 0$ were used at the borders. A mesh of 8000 elements was used, and the simulation was performed at 81 frequencies from 10 kHz to 1 GHz. The grid convergence showed that the element count is sufficient. Gas parameters for air in Table I were used in the simulations.

B. Validity of the compact model

Several numerical simulations were performed to be able to test the validity and accuracy of the compact model for the 1D squeeze-film damper derived in the previous section. Here, the accurate model for the air gap region in Appendix A is used. Table II summarizes the dimensions of all simulated damper topologies. The simulated topologies were limited to cases where the ratio $l_x/h_0 \geq 10$. With smaller ratios the zero pressure border condition is not justified. Also, the pressure is no more constant across the gap even at small frequencies. These phenomena have been studied in [12]

TABLE II
DIMENSIONS OF THE SIMULATED DAMPERS

Length l_x [μm]	Gap h_0 [μm]	x-resonance $f_{x,2}$ [MHz]	z-resonance 1 $f_{z,1}$ [MHz]	z-resonance 2 $f_{z,2}$ [MHz]
5	0.5	-	168.4	
5	1	22.8	83.9	172.4
10	0.5	-	168.4	329
10	1	-	83.84	168.4
10	2	14.4	40.82	85.6
15	0.5	-	176.5	337
15	1	-	81.96	172.4
15	2	8.41	71.78	85.9
15	3	10.1	28.8	52.2
20	0.5	-	167.5	329
20	1	-	88.0	169
20	2	4.58	42.0	85.3
20	3	7.21	29.0	58.3

Figure 4 compares frequency responses of numerical and compact models in a case when $l_x = 20\,\mu$m and $h_0 = 2\,\mu$m. The simulated data is presented in two forms: (a) amplitude/phase of the impedance Z_m, and (b) damping/spring coefficients. Both responses show that the compact model response is very accurate at low and high frequencies, but there is a noticeable error in the compact model just below the first gap resonance frequency. This was expected, since this

 ISBN: 978-2-35500-006-5

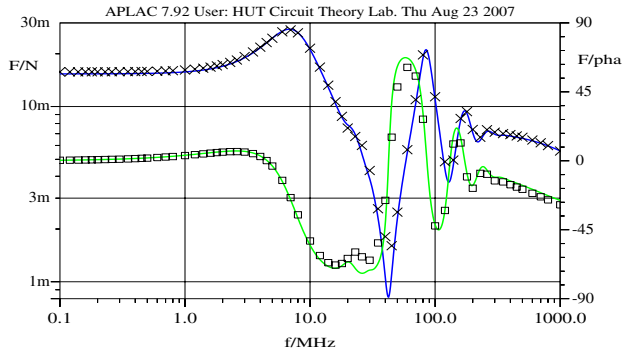

(a)

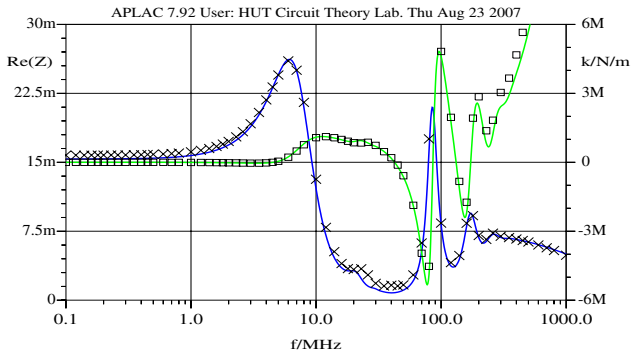

(b)

Fig. 4. Simulated frequency responses of the numerical model (×, □) and the new compact model (solid lines). Here $l_\mathrm{x} = 20\,\mu$m and $h_0 = 2\,\mu$m. (a) magnitude (×) and phase (□) of the impedance, (b) damping coefficient $c = \Re(Z_\mathrm{m})$ (×) and the spring coefficient $k = -\Re(\mathrm{i}\omega Z_\mathrm{m})$ (□).

regime is between the squeeze-film and the gap resonance regions.

Table II summarizes the resonant frequencies detected from the amplitude/phase responses of all simulated topologies. Here, the resonant frequencies are those where the phase of the impedance crosses zero.

To see the validity of the resonant frequency approximations in (8) and (9), they are compared with the results in Table II. The effective speed of sound propagating in the gap is

$$c_\mathrm{e} = c_0\sqrt{\frac{5(1+2K_\mathrm{s})}{6\gamma}} \tag{33}$$

The fundamental resonant frequencies $f_{\mathrm{x},2}$ and $f_{\mathrm{z},1}$ become $6.94\,$MHz and $43.52\,$MHz respectively, for a topology of a width of $20\,\mu$m and gap height of $2\,\mu$m.

IV. Conclusions

With these models, the Reynolds equation has been extended to be applicable to rapidly oscillating surfaces and rarefied gas conditions in addition to modelling damping at low frequencies. It was shown that the compact model is in good agreement with numerical FEM simulation results. Slip conditions are used to have an accurate model also for small air gaps typical in MEMS devices.

In this study, idealistic border conditions for the damper borders were assumed. These conditions are not justified in cases where the aspect ratio (l_x/h_0) is not small. To model accurately such cases, the flow outside the gap should be considered [12]. It is straightforward to extend the approach to 2D squeeze damper topology considering the y dimension.

The solver for viscous acoustic flow in the Elmer software [10] turned out to be very useful in studying the squeeze-film phenomena at the high frequency regime.

References

[1] J. W. Wang, Z. Ren, and C. T.-C. Nguyen, "1.156-GHz Self-Aligned Vibrating Micromechanical Disk Resonator," *IEEE Transactions on Ultrasonics, Ferroelectrics, and Frequency Control*, vol. 51, no. 12, pp. 1607–1628, 2004.

[2] J. Wang, J. E. Butler, T. Feygelson, and C. T.-C. Nguyen, "1.51-GHz Nanocrystalline Diamond Micromechanical Disk Resonator With Material-Mismatched Isolating Support," *IEEE Micro Electro Mechanical Systems Conference*, (Maastricht, The Netherlands), pp. 641–644, January 2004.

[3] J. J. Blech, "On Isothermal Squeeze Films," *Journal of Lubrication Technology*, vol. 105, pp. 615–620, October 1983.

[4] W. S. Griffin, H. H. Richardson, and S. Yamanami, "A Study of Fluid Squeeze-Film Damping," *Journal of Basic Engineering, Trans. ASME*, vol. 88, pp. 451–456, June 1966.

[5] T. Veijola, "Compact Models for Squeezed-Film Dampers with Inertial and Rarefied Gas Effects," *Journal of Micromechanics and Microengineering*, vol. 14, pp. 1109–1118, 2004.

[6] W. M. Beltman, P. J. van der Hoogt, R. M. E. J. Spiering, and H. Tijdeman, "Air Loads on a Rigid Plate Oscillating Normal to Fixed Surface," *Journal of Sound and Vibration*, vol. 206, pp. 217–241, 1997.

[7] W. M. Beltman, "Viscothermal Wave Propagation Including Acousto-Elastic Interaction, Part I: Theory," *Journal of Sound and Vibration*, vol. 227, pp. 555–586, 1999.

[8] T. Veijola and A. Lehtovuori, "Model for Gas Damping in Air Gaps of RF MEMS Resonators," *Symposium on Design, Test, Integration and Packaging of MEMS/MOEMS, DTIP 2007*, (Stresa, Italy), pp. 156–161, April 2007.

[9] M. Malinen, M. Lyly, P. Råback, A. Kärkkäinen, and L. Kärkkäinen, "A Finite Element Method for the Modeling of Thermo-Viscous Effects in Acoustics," *Proceedings of the 4th European Congress on Computational Methods in Applied Sciences and Engineering* (P. Neittaanmäki, T. Rossi, K. Majava, and O. Pironneau, eds.), (Jyväskylä, Finland), July 2004.

[10] Elmer, "Elmer – Finite Element Solver for Multiphysical Problems," 2006. http://www.csc.fi/elmer.

[11] G. E. Karniadakis and A. Beskok, *Micro Flows, Fundamentals and Simulation*. Springer, Heidelberg, 2002.

[12] T. Veijola, A. Pursula, and P. Råback, "Extending the Validity of Existing Squeezed-Film Damper Models with Elongations of Surface Dimensions," *Journal of Micromechanics and Microengineering*, vol. 15, pp. 1624–1636, 2005.

[13] A. Burgdorfer, "The Influence of the Molecular Mean Free Path on the Performance of Hydrodynamic Gas Lubricated Bearings," *Journal of Basic Engineering, Trans. ASME*, vol. 81, pp. 94–99, March 1959.

 ISBN: 978-2-35500-006-5

APPENDIX A

An exact solution for (12) – (15) is presented considering the non-adiabatic thermal conditions and boundary conditions for velocity and temperature. After some manipulation, the following fourth order differential equation results

$$\frac{1}{s^2\phi^2}\left(\frac{1}{\mathrm{i}k}+\frac{4k\gamma}{3s^2}\right)w''''-\left(\frac{\mathrm{i}4k}{3s^2}+\frac{\mathrm{i}k\gamma}{s^2\phi^2}+\frac{1}{k}\right)w''-kw=0 \tag{A1}$$

for velocity w and

$$\frac{1}{s^2\phi^2}\left(\frac{1}{\mathrm{i}k}+\frac{4k\gamma}{3s^2}\right)T''''-\left(\frac{\mathrm{i}4k}{3s^2}+\frac{\mathrm{i}k\gamma}{s^2\phi^2}+\frac{1}{k}\right)T''-kT=0 \tag{A2}$$

for temperature T as well. In this Appendix, the derivatives with the respect to z are denoted with primes ($T'''' = \partial^4 T/\partial z^4$), and the dependence on z is denoted by, e.g., $w(z)$ or $T''(z)$. These homogenous linear equations with constant complex coefficients have a characteristic equation $\alpha_1 r^4+\alpha_2 r^2-k=0$, where

$$\alpha_1 = \frac{1}{s^2\phi^2}\left(\frac{1}{\mathrm{i}k}+\frac{4k\gamma}{3s^2}\right) \tag{A3}$$

$$\alpha_2 = -\left(\frac{\mathrm{i}4k}{3s^2}+\frac{\mathrm{i}k\gamma}{s^2\phi^2}+\frac{1}{k}\right) \tag{A4}$$

The roots of the characteristic equation are

$$r_1 = \sqrt{\frac{-\alpha_2+\sqrt{\alpha_2^2+4\alpha_1 k}}{2\alpha_1}},\ r_3=-r_1 \tag{A5}$$

$$r_2 = \sqrt{\frac{-\alpha_2-\sqrt{\alpha_2^2+4\alpha_1 k}}{2\alpha_1}},\ r_4=-r_2 \tag{A6}$$

and thus the solution of (A1) is

$$w(z)=C_1e^{r_1z}+C_2e^{r_2z}+C_3e^{r_3z}+C_4e^{r_4z}. \tag{A7}$$

Constants C_1, C_2, C_3, and C_4 are determined using boundary conditions:

$$w(0) = 0, \qquad w(1)=w_0, \tag{A8}$$

$$T(0) = K_{\mathrm{T}}T'(0), \quad T(1)=-K_{\mathrm{T}}T'(1). \tag{A9}$$

Therefore, the temperature is written as function of velocity w. Equations (12) – (15) reduce now to

$$T' = A_1w+A_2w'' \tag{A10}$$

$$w' = A_3T+A_4T'', \tag{A11}$$

where

$$A_1 = -\mathrm{i}k\gamma, \tag{A12}$$

$$A_2 = \left(\frac{1}{\mathrm{i}k}+\frac{4k\gamma}{3s^2}\right), \tag{A13}$$

$$A_3 = -\frac{\mathrm{i}k}{\gamma-1}, \tag{A14}$$

$$A_4 = \frac{k\gamma}{(\gamma-1)s^2\phi^2}. \tag{A15}$$

Solving T from (A10) and (A11) and p from (5), (6) and (A16) yields

$$T = B_1w'+B_2w''', \tag{A16}$$

$$p = -\frac{1}{\mathrm{i}k}w'+T=\left(B_1-\frac{1}{\mathrm{i}k}\right)w'+B_2w''' \tag{A17}$$

where B_1 and B_2 are the auxiliary variables:

$$B_1=\frac{1-A_1A_4}{A_3},\ B_2=-\frac{A_2A_4}{A_3}. \tag{A18}$$

Equation (A16) can be used to utilize the boundary conditions for temperature in (A9) to solve the velocity:

$$\begin{aligned} B_1w'(0)+B_2w'''(0) &= K_{\mathrm{T}}B_1w''(0)+K_{\mathrm{T}}B_2w''''(0),\\ B_1w'(1)+B_2w'''(1) &= -K_{\mathrm{T}}B_1w''(1)-K_{\mathrm{T}}B_2w''''(1). \end{aligned}$$

After applying boundary conditions for velocity in (A8) in addition to the conditions above, the following system of equations results:

$$C_1+C_2+C_3+C_4=0, \tag{A19}$$

$$C_1e^{r_1}+C_2e^{r_2}+C_3e^{r_3}+C_4e^{r_4}=w_0, \tag{A20}$$

$$C_1Q_1+C_2Q_2+C_3Q_3+C_4Q_4=0, \tag{A21}$$

$$C_1S_1e^{r_1}+C_2S_2e^{r_2}+C_3S_3e^{r_3}+C_4S_4e^{r_4}=0, \tag{A22}$$

where $Q_i=(B_1r_i+B_2r_i^3)(1-K_{\mathrm{T}}r_i)$ and $S_i=(B_1r_i+B_2r_i^3)(1+K_{\mathrm{T}}r_i)$. Solving the system of equations (A19)–(A22) gives the coefficients C_i in (A7) which are

$$C_1 = \frac{H_2P_3M-GP_3-MP_2}{P_1+P_2L-H_1P_3-H_2P_3L}, \tag{A23}$$

$$C_2 = LC_1+M, \tag{A24}$$

$$C_3 = G-H_1C_1-H_2C_2, \tag{A25}$$

$$C_4 = -C_1-C_2-C_3, \tag{A26}$$

where

$$G = w_0/(e^{r_3}-e^{r_4}), \tag{A27}$$

$$H_1 = (e^{r_1}-e^{r_4})/(e^{r_3}-e^{r_4}), \tag{A28}$$

$$H_2 = (e^{r_2}-e^{r_4})/(e^{r_3}-e^{r_4}), \tag{A29}$$

$$L = \frac{H_1K_3-K_1}{K_2-H_2K_3}, \tag{A30}$$

$$M = \frac{-GK_3}{K_2-H_2K_3}, \tag{A31}$$

$$\begin{aligned} K_i &= B_1(r_i-r_4)+B_2(r_i^3-r_4^3)\\ &- K_{\mathrm{T}}B_1(r_i^2-r_4^2)-K_{\mathrm{T}}B_2(r_i^4-r_4^4), \end{aligned} \tag{A32}$$

$$\begin{aligned} P_i &= B_1(r_ie^{r_i}-r_4e^{r_4})+B_2(r_i^3e^{r_i}-r_4^3e^{r_4})\\ &+ K_{\mathrm{T}}B_1(r_i^2e^{r_i}-r_4^2e^{r_4})\\ &+ K_{\mathrm{T}}B_2(r_i^4e^{r_i}-r_4^4e^{r_4}). \end{aligned} \tag{A33}$$

Now the values for variables $p(z)$, $w(z)$, $T(z)$ can be calculated from (A17), (A7) and (A16), respectively. The density is simply $\rho(z)=p(z)-T(z)$.

 ISBN: 978-2-35500-006-5